Laser light sheet profile and alignment effects on PIV performance

K. Grayson[1,*], C. M. de Silva[1], N. Hutchins[1], I. Marusic[1]
1: Dept. of Mechanical Engineering, University of Melbourne, Australia
* Correspondent author: kgrayson@student.unimelb.edu.au

Keywords: Particle image velocimetry, laser diagnostics, PIV uncertainties, wall-bounded turbulence

ABSTRACT

The sensitivity and impact of laser profile misalignment and shape mismatch on Particle Image Velocimetry (PIV) measurements are investigated in this study. While the effects of laser profile misalignment can be equivalent to an out-of-plane velocity component, light sheet mismatch can be identified and corrected prior to an experiment, decreasing PIV uncertainties. Synthetic particle image simulations are used to isolate and systematically vary laser profile mismatch parameters between successive PIV laser pulses. Two simulation cases are discussed, analysing the effects of a misalignment between two otherwise identical laser pulses, as well as a mismatch in the width of two laser profiles. Our results reveal a steady degradation in mean correlation coefficient as the laser profiles are increasingly mismatched in shape and alignment, coupled with a rapid rise in the detection of spurious vectors. These findings reinforce the need to consider laser sheet alignment and intensity distribution when seeking to capture high quality PIV measurements. The design of a modular and inexpensive laser profiling camera is outlined to enable robust and repeatable quantification of laser sheet overlap and beam characteristics. The profiling system is also found to be a valuable tool for laser diagnostics and aiding the setup of experiments. Various potential applications of this device are presented for PIV and other laser-based measurement techniques. Finally, preliminary results from PIV experiments which involve the deliberate misalignment of laser profiles are discussed. These data reiterate the trends observed in simulations, but also emphasise the coupled complexity of laser profile mismatch behaviour in experimental scenarios, placing the idealised simulation results in some context. Collectively, our findings highlight the importance of well-matched laser profiles. A more rigorous experimental quantification of these behaviours has the potential to enhance the quality of PIV results.

1. Introduction

The shape and alignment of laser beam profiles can have a large influence on the quality of results from laser-based flow visualisation techniques. Particle Image Velocimetry (PIV) is particularly reliant on the alignment and similarity of laser beam profiles from each pulsed laser cavity in order to achieve good correlation of experimental image pairs. Therefore quantifying and refining laser overlap and profile distributions can help to improve experimental results, particularly when performing experiments with multiple pulses (3 or 4 pulse PIV) and larger fields of view.

The effects of two misaligned, but otherwise identical light sheets in a PIV experiment are equivalent to an out-of-plane velocity component in the flow (see figure 1), increasing the out-of-plane loss of particle pairs under typical flow conditions (Scharnowski & Kähler 2016). Under extreme out-of-plane velocity conditions, this behaviour may even be exploited to minimise out-of-plane loss of pairs by deliberately misaligning laser sheets (Kähler & Kompenhans 2000). A number of studies have investigated the effects of out-of-plane loss of pairs on PIV results and the impact on PIV uncertainties (Nobach & Bodenschatz 2009, Nobach 2011, Scharnowski & Kähler 2016). However, while out-of-plane velocity components may be unavoidable in a given flow of interest, laser light sheet mismatch can be identified and corrected prior to performing an experiment. This correction of the experimental setup prior to capturing PIV images decreases the uncertainty associated with the measurement, yielding higher quality results.

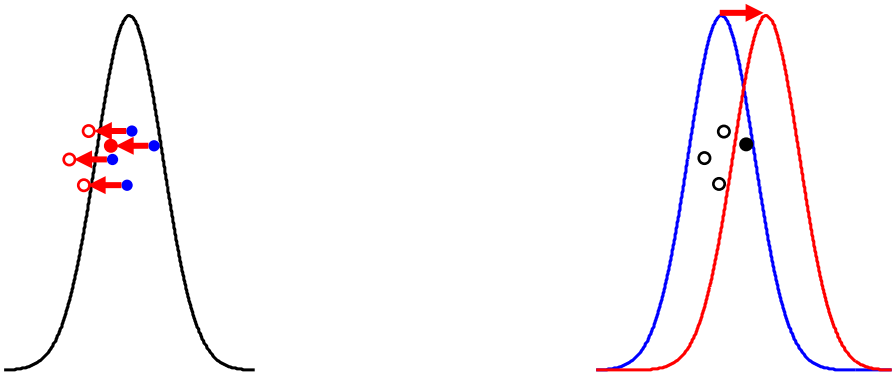

(a) (b)

Fig. 1 (a) Out-of-plane loss of particle pairs due to out-of-plane velocity component, (b) Out-of-plane loss of particle pairs due to laser light sheet misalignment

Despite the importance of laser light sheet overlap and the similarity of laser profiles for high quality PIV measurements, tuning laser shape and alignment is rarely discussed explicitly in PIV publications. Many experimental papers neglect any mention of light sheet parameters and behaviour, while others may mention a light sheet thickness without any explanation for the measurement method or width criteria used to define what is often assumed to be a Gaussian profile. We note that laser sheet thicknesses can be extracted from stereo PIV measurements (Wieneke 2005) and tomographic PIV allows an approximation of the laser sheet intensity distribution to be reconstructed (Blinde et al. 2015). However, more detailed measurements of

the laser sheet in stereo and tomographic PIV configurations, as well as any laser measurements for 2D PIV setups, require a more rigorous approach.

Some studies do make an effort to control and specify the laser thickness by employing a fixed-width slit, which forces a top-hat light sheet profile. Assuming negligible laser beam divergence, the laser sheet thickness is therefore equal to the slit width (Scarano et al. 2006, Elsinga et al. 2006, Blinde et al. 2015). This method however does not account for variations in laser intensity distribution or overlap. Laser burn tests can be a useful method of comparing light sheet thickness and estimating sheet separations, and this method was used in a dual-plane PIV study by Ganapathisubramani et al. (2005). However burn papers generally offer insufficient resolution and dynamic range to analyse the sheet intensity distribution in detail. Imaging a surface illuminated by a laser sheet can yield further information regarding the intensity distribution. Fond et al. (2015) imaged sampled laser sheets with a piece of paper normal to the laser beam, while Kähler & Kompenhans (2000) and Mistry & Dawson (2014) imaged the sheet on a white plate, inclined relative to the laser sheet for increased resolution. Electronic laser profiling methods are increasingly being used to quantify laser intensity distributions and alignment with greater sensitivity and repeatability. Studies have used a knife edge laser profiler (Mullin & Dahm 2005), laser profiles of the laser beam prior to manipulation by the sheet optics (Brücker et al. 2012), and camera based laser profilers for monitoring laser sheet distributions and alignment (Mullin & Dahm 2005, Pfadler et al. 2009, Naka et al. 2016). Camera based laser profilers tend to offer the greatest flexibility with typical pulsed PIV lasers, since they are able to easily capture dynamic, as well as static, laser beam behaviours.

Commercial camera-based laser profiling devices, such as that used by Naka et al. (2016), are available to measure laser beam distributions and alignments, but are expensive and can lock users into closed, proprietary software packages and image formats. They also may not be totally 'ready-to-run' – it is likely additional optics will be required to attenuate the high power laser beams used routinely in PIV measurements. At the opposite end of the cost spectrum however, researchers are using modified webcams for beam alignment and profiling with great success (Cignoli et al. 2004, Andrèbe et al. 2011, Langer et al. 2013). Webcams offer an extremely low cost, off-the-shelf means of measuring laser beam profiles, requiring only the removal of their camera lens and the addition of attenuating optics to operate. This configuration has been demonstrated in applications from Laser Induced Fluorescence measurements to lasers used in fusion reactors (Cignoli et al. 2004, Andrèbe et al. 2011).

This study examines the impact of laser sheet misalignment and profile mismatch in PIV experiments with the simulation of particle images, estimating the sensitivity of laser configurations on PIV measurement quality. The design of a modular, low-cost laser profiling device will also be outlined to aid the quantification and correction of these effects in laboratory experiments. Measurements from this camera are then used to compare experimental laser misalignments to the simulated and predicted behaviours.

Throughout this paper, the coordinate system x, y and z refers to the streamwise, spanwise and wall-normal directions respectively. Corresponding instantaneous streamwise, spanwise and wall-normal velocities are denoted by u, v and w. Overbars indicate averaged quantities, and a superscript + refers to normalisation by inner scales, where $u^+ = u/u_\tau$ and u_τ defines the friction velocity.

2. Simulating Laser Sheet Mismatch

The effects of laser sheet mismatch can be systematically investigated with the use of simulated PIV images, generated from Direct Numerical Simulation (DNS) datasets. This enables control over all measurement parameters, such that variables of interest can be isolated and their impacts examined in detail.

Simulation Methodology

The simulations performed in this study use an in-house PIV simulation and processing Matlab code, originally developed for Tomographic PIV simulations (see de Silva et al. 2012). This program has since been modified for 2D planar PIV simulations with increased functionality. These improvements include more rigorous modelling of PIV image noise behaviours, uniform and non-uniform Gaussian light sheet profiles, particle non-uniformities, imperfect camera focus and loss of sharpness at the edges of a synthetic image. Collectively, these features allow the generation of less 'ideal' and more experimentally realistic PIV images for analysis.

The simulation procedure uses DNS velocity fields to displace randomly located virtual particles and generate synthetic PIV particle images. These images are then fed into a PIV processing and correlation code. The resulting velocity fields can then be directly compared to the DNS velocity fields and errors can be calculated. Using this method, the degree of laser light sheet overlap can be systematically varied and comparisons between the synthetic PIV velocity fields can be made.

Simulation Parameters

For the present study, the turbulent boundary layer DNS dataset from Sillero et al. (2013) at Re_θ = 6500 is used. Synthetic two-pulse, 16-bit particle images are generated over a streamwise-spanwise plane, with a simulated Gaussian light sheet profile. A DNS domain of 4200 × 6300 viscous units (streamwise × spanwise) is applied with a 1.6 viscous unit/pixel resolution at a wall normal height of approximately 240 viscous units. Infinite depth of field and no image noise is modelled in this simulation, while experimentally representative particle sizes and size variations are used. A multipass algorithm with window deformation is used to process the resulting synthetic images from a 64 × 64 pixel interrogation window down to a final interrogation window size of 32 × 32 pixels, or approximately 20 × 20 viscous units. Results are averaged over ten distinct DNS flow fields, as well as over cases that interchangeably misalign pulse 1 (with pulse 2 fixed), and misalign pulse 2 (with pulse 1 fixed), in order to avoid biasing effects.

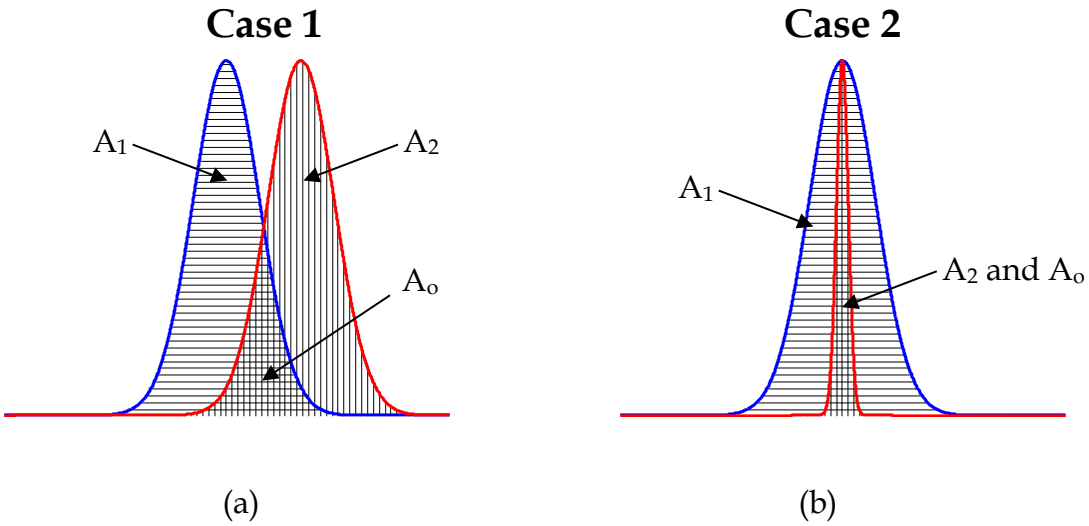

Fig. 2 (a) Extreme case 1 shift tested (37.5% shift), (b) Extreme case 2 width mismatch tested (1.3/7.1 viscous unit standard deviations). Horizontal hatching denotes profile area A_1, while the vertical hatching denotes profile area A_2. Cross-hatched regions indicate areas of profile overlap, quantified by area A_o.

Two separate laser mismatch scenarios are considered. In case 1, two identical Gaussian light sheet profiles are systematically translated relative to one-another, shown schematically in figure 2(a). This scenario is directly equivalent to the presence of an out-of-plane flow velocity component. The Gaussian light sheet thickness used in this simulation case remains fixed, with a standard deviation of 7.1 viscous units. This thickness was determined by performing a

Gaussian fit onto a representative experimental light sheet profile. Light sheet misalignment is simulated in scenarios ranging from perfect overlap to a shift equivalent to 37.5% of the $\pm 3\sigma$ light sheet width.

Case 2 investigates the impact of different light sheet widths on PIV performance, shown in figure 2(b). In this scenario, both laser pulses remain centred about a fixed location, but the standard deviation of one Gaussian light sheet profile (from one laser pulse) is varied, while the other light sheet profile (from the other laser pulse) remains fixed. Scenarios have been simulated with Gaussian laser profile standard deviations ranging from 1.3 viscous units to 7.1 viscous units, while the fixed light sheet profile uses a constant standard deviation of 7.1 viscous units. Therefore the misaligned case always has a narrower laser sheet profile than the reference 7.1 viscous unit standard deviation case.

Simulation Results

In order to compare the results of cases 1 and 2 on a common axis, the area ratio of the laser profile overlap (A_r) is defined in equation (1).

$$A_r = \frac{A_o}{\max(A_1,\ A_2)} \qquad (1)$$

A_1 and A_2 are the areas beneath PIV laser profiles 1 and 2 respectively, illustrated by the horizontal and vertical hatching in figure 2. A_o represents the overlapping area of the two laser profiles, shown by the cross-hatched regions in figure 2. Note that in figure 2(b), profile 2 is fully contained within profile 1 and consequently A_o is equivalent to A_2. Using this metric, an area ratio of 100% indicates that the two laser profiles are identical in both shape and alignment. In contrast, an area ratio of 0% implies that the two laser profiles do not overlap whatsoever.

Figure 3(a) shows the normalised average correlation coefficient ($\bar{R}_C/\bar{R}_{C,max}$) calculated for an unfiltered velocity field for both simulation cases 1 and 2. $\bar{R}_C$ is computed by averaging the correlation coefficient (over the range [0 1]) across the entirety of each simulation correlation field. These results show a steady degradation of mean correlation coefficient for both case 1 (blue squares) and case 2 (red circles), that begins to fall away more rapidly with $A_r < 70\%$. Furthermore, the mean correlation coefficient of case 2 does not drop as quickly as case 1. This observation may be attributed to case 2's symmetric change in width about the mean. So, while fewer particles are illuminated by the "narrow" light sheet pulse (and a drop in particle density degrades correlation), the proportion of particle pairs between image 1 and 2 should remain high since the thicker laser sheet can compensate for moderate out-of-plane velocities. The interaction

therefore between two pulsed laser sheets' alignment and thickness (as well as the shape of their profile, which is beyond the scope of the current study) is reasonably complex, influencing not only the particle image pairs but interrogation window particle densities and variations in particle image intensities.

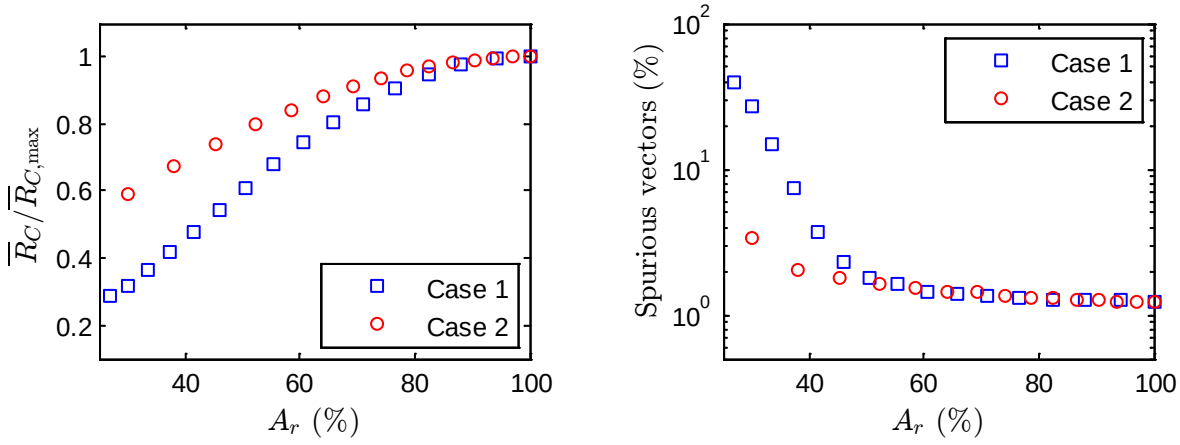

(a) (b)

Fig. 3 (a) Normalised mean correlation coefficient of simulation test cases, (b) Percentage of spurious vectors detected on linear-log axes

The simulation results from both cases 1 and 2 can also be filtered like any typical PIV experiment data to check for and remove spurious vectors. To this end, Westerweel and Scarano's normalised median test (Westerweel & Scarano 2005) was applied to these results, using the recommended threshold and epsilon values of 2.0 and 0.1 pixels for all scenarios. The resulting percentage of spurious vectors detected from the velocity vector fields in different laser sheet shift and width mismatch scenarios is shown on linear-log axes in figure 3(b). The results show that both case 1 and 2 simulations with high overlap area ratios ($A_r > 60$) contain few spurious vectors, consistent with their reasonably well aligned and matched laser profiles. However the proportion of spurious vectors detected by the normalised median test increases rapidly for area ratios less than 50%. These correspond to simulations where the shift is greater than 23% of the Gaussian's $\pm 3\sigma$ width (case 1) or when the width of one laser sheet profile is 3.5 times greater than the other (case 2). While it is conceivable that mismatched laser sheet thicknesses by a factor of 3.5 could be identified using conventional alignment methods such as burn tests, a 23% shift misalignment of the laser profiles is more subtle and detection is less likely. For experiments with a laser sheet thickness on the order of 1mm, a 23% sheet misalignment constitutes an offset of just 0.23mm. A laser sheet misalignment of this order

under experimental conditions would be difficult to identify and correct using burn tests or visual alignment methods. Furthermore, very small changes in laser sheet alignment around the spurious vector threshold ($A_r = 50\%$) have large consequences for the proliferation of spurious vectors. Changing the area ratio from 50% to 40% almost doubles the proportion of spurious vectors detected (from 5.9% to 11.4%), and only involves an increase in the pulse shift (case 1) from 23% to 28% (or an additional misalignment of 0.05mm for a 1mm thick laser sheet). A misalignment of this magnitude could therefore be the difference between noisy, but acceptable PIV measurements, and effectively unusable datasets.

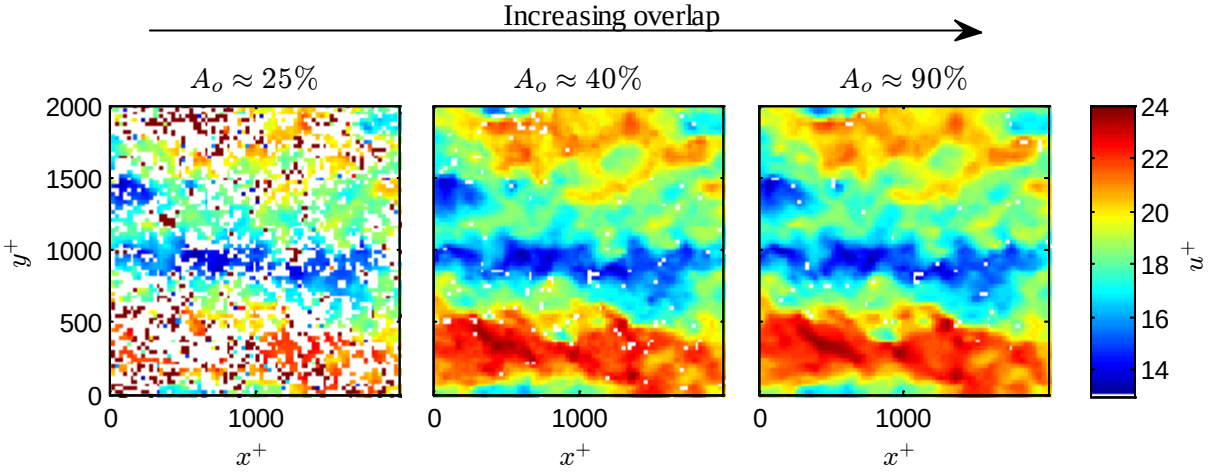

Fig. 4 Median test filtered streamwise velocity fields from case 1 simulations. The streamwise and spanwise dimensions are denoted by x and y respectively.

Figure 4 illustrates the consequences of laser misalignment and mismatch on instantaneous streamwise velocity fields after the application of the normalised median test. Case 1 simulations are compared with area ratios of 90% (near 'ideal', or a shift of 5%), 40% (around the spurious vector threshold), and 25% (well beyond the spurious vector threshold). The white gaps in the field represent spurious vectors that have been detected and omitted. While the parameters of the median test could certainly be refined to better filter the $A_r \approx 25\%$ field and remove the obvious remaining spurious vectors, the high proportion of omitted vectors would make such a velocity field near unusable. It is also worth noting that even though we do not see a sharp increase in the number of spurious vectors until $A_r < 50\%$, we anticipate that the error associated with the computed velocities and other flow statistics will be significantly higher, even at moderately high A_r.

When considering these simulation results, it is important to recognise that they do not model many variables present in physical PIV experiments that will have an impact on measurement performance. Both laser pulses are assumed to have identical Gaussian laser sheet profiles, which is highly unlikely to be the case in real PIV experiment scenarios. Modelling CCD noise and other undesirable image effects would also decrease the quality of correlations and increase the proportion of spurious vectors, which may lead to amplified issues associated with non-ideal laser overlap. These results can therefore be considered a 'best case' scenario for the consequences of poor laser alignment and profile matching, since additional realities of PIV experiments are only likely to increase the impact of these effects. Good laser sheet alignment and well matched laser sheet profiles can be critically important for quality PIV measurements.

3. Laser Profiling Camera

Camera Configuration

In order to correct laser alignment and profile issues, a modular, low cost laser profiling device is proposed. This laser profiler uses a mirrorless interchangeable lens camera with a large APS-C size sensor measuring 22.3 × 14.9mm^2, able to comfortably fit the unfocused laser beams used in typical PIV experiments. A Canon EOS-M camera body was used for this purpose (no lens is required), containing an 18 megapixel sensor that results in a pixel density of ~230px/mm (see item #5 in figure 5(b)). A wired remote trigger is used with a Wi-Fi enabled SD card to remotely capture and review images in near real-time.

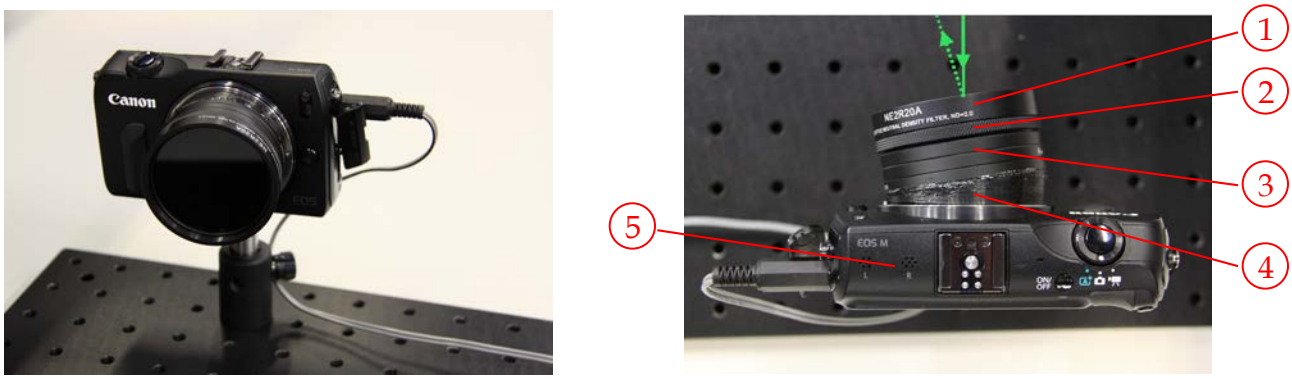

(a) (b)

Fig. 5 (a) The laser profiling camera setup, (b) Top annotated view of laser profiling camera

Due to sensitive electronics within digital cameras, attenuation optics are needed to image a laser profile without damaging the camera sensor. These optics also require the flexibility to adjust filter strength in order to tune image exposure for different setups and laser powers. In this study, as with prior published works (Cignoli et al. 2004, Langer et al. 2013), neutral density

filters are used to achieve the necessary attenuation. These optics are commonly available with threaded mounts and in a variety of strengths to be stacked, mixed and matched. The laser profiling setup uses a combination of laser-grade neutral density filters and standard photographic neutral density filters used for still photography. Laser-grade neutral density filters are ideal for this application, purpose built to take energy densities found in laser profiling. Photographic neutral density filters however have the advantage of being inexpensive and readily available in a variety of filter strengths. They are also capable of withstanding a surprising amount of laser energy. The profiling setup in this study uses a variety of photographic neutral density filters of different strengths (item #3 in figure 5(b)), and a laser-grade neutral density filter is added to the top of the filter stack via a threaded adapter (items #1 and #2 in figure 5(b)) when profiling higher energy laser beams (such as 400mJ/pulse 532nm beams).

These filters thread onto a metal filter step ring that is epoxied to a 3D printed camera lens mount (item #4 in figure 5(b)). This mount locks into the camera as required and angles the filters off the sensor plane to prevent any laser reflections returning through the beam path into the laser unit and causing damage. An overview of this setup is shown in figure 5(b), where the solid green line shows the incident path of a sampled laser beam and the dotted green line indicates the direction of any surface reflections off the neutral density filters.

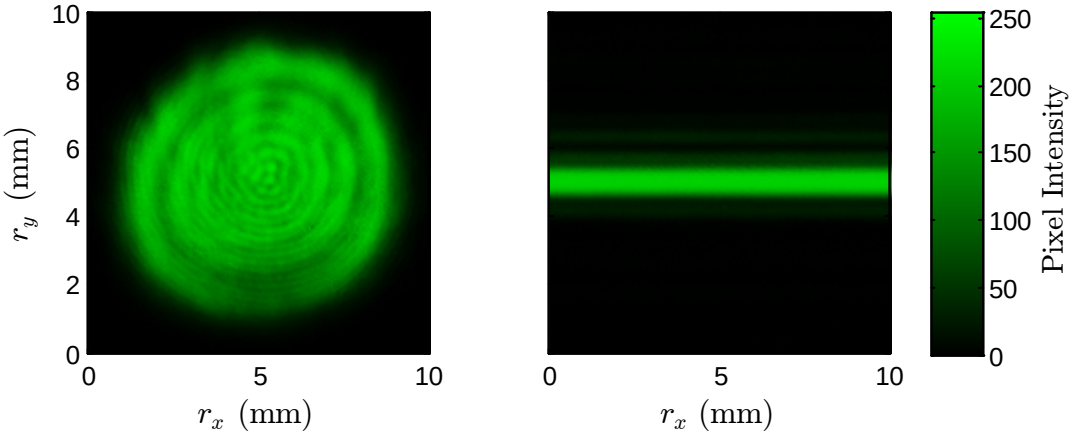

(a) (b)

Fig. 6 (a) An imaged laser beam profile, (b) A captured laser light sheet profile. r_x and r_y correspond to the horizontal and vertical laser profile dimensions in physical space.

Figure 6(a) shows a sample laser beam profile captured with the device. We note the pattern of concentric rings is considered typical of this particular Nd:YAG laser. However a slight asymmetry of the beam can also be identified in this image that is difficult to observe in many burn tests, with the top of the profile slightly brighter than the bottom. This asymmetry can have significant consequences when the beam is spread into a laser sheet for PIV, and can cause asymmetric or multi-lobed laser sheet profiles. Figure 6(b) shows a laser sheet profile from a similar 532nm Nd:YAG laser.

Camera Applications

This laser profiling camera has numerous potential applications for laser tuning, diagnostics and experimental setup. Profiling a laser beam can reveal non-uniformities in the beam profile, overlap issues and reveal potential faults in the laser unit. Regular measurements of beam profiles can also monitor incremental degradation of laser performance and inform service schedules for laser equipment. Dynamic laser behaviours such as the time required for the laser to warm up and reach thermal equilibrium from a cold start, or shot to shot beam stability have been recognised as important factors when performing PIV experiments (Kähler & Kompenhans 2000, Fond et al. 2015). A camera-based laser profiler, such as the device discussed in this study, is capable of quantifying and monitoring these behaviours in a given laser unit, which will be the subject of future work.

Laser light sheets can also be profiled with this device (see figure 6(b)), and measurements such as these can be crucial to ensuring well matched laser sheet profiles for PIV images. The alignment and intensity distributions of the light sheet can be quantified across the measurement region to optimise PIV image quality over the entire field of view.

Furthermore, this laser profiling system is not restricted to use with PIV equipment, it can be used with a large range of experiments involving laser devices. Tests with this setup have also been performed on a Laser Doppler Anemometry system to verify laser stability, profiles and laser crossover locations and symmetry. To date, this device has captured data from 120mJ/pulse up to 400mJ/pulse Nd:YAG 532nm pulsed PIV lasers, as well as continuous ~90mW 660nm red and 785nm infrared laser beams.

4. Experimental Laser Misalignment

A PIV experimental dataset involving deliberate mismatching of the laser light sheet has been captured to compare experimental behaviours with the simulation results outlined in Section 2. This study presents the preliminary results from the experiment and simulation comparison.

Two pulse, 2D PIV measurements were taken of a Re_θ = 7500 (approx.) turbulent boundary layer in the High Reynolds Number Boundary Layer Wind Tunnel (HRNBLWT) at the University of Melbourne (for further details regarding this facility, see Nickels et al. 2005). Data was captured in the streamwise-spanwise plane over a region measuring 4200 × 6300 viscous units (streamwise × spanwise), and at a wall normal height of approximately 240 viscous units. Additional details regarding the features of this experimental PIV configuration can be found in de Silva et al. (2015). PIV images were captured using a single 11 megapixel PCO 4000 PIV camera and a Nikon AF Micro-Nikkor 60mm 2.8D lens, providing an image resolution of 2672 × 4008 pixels (streamwise × spanwise) and a flow resolution of approximately 1.6 viscous units/pixel. Note that the experimental field of view and spatial resolution in viscous units are effectively identical to that considered by the simulations outlined in Section 2 (with only negligible variations between the two cases). A Spectra-Physics Quanta-Ray PIV-400 pulsed 532nm Nd:YAG laser (nominally at 400mJ/pulse) was used over a 10m beam path to generate the laser sheet. Seeding was provided by polyamide particles.

The beam combining optics of the Spectra-Physics PIV-400 laser used in this experiment are readily accessible in the front of the laser unit. Therefore, measurements were taken by misaligning the laser beam using the combining optics, and then allowing the laser and wind tunnel to stabilise before capturing a set of 120 PIV image pairs. This process was repeated several times to obtain a variety of laser alignment combinations.

Preliminary results from these measurements are shown in figure 7, which plots the area ratio (A_r) versus normalised average correlation coefficient ($\bar{R}_C/\bar{R}_{C,max}$) of the experimental data. The average correlation coefficient ($\bar{R}_C$) of the experimental data was calculated over a representative strip of the average correlation field which coincided with the laser profiling measurement location (used to calculate A_r). For consistency, $\bar{R}_{C,max}$ is matched to that of the simulation results shown in figure 3(a). The results in figure 7 exhibit the same trend as found with the simulations, where lower A_r corresponds with lower average correlation coefficient. However, it is noted that the forced misalignments implemented in experiments do not maintain the ideal laser mismatch behaviours tested in simulation cases 1 and 2. Instead, an experimental shift in the alignment of

one laser pulse is typically coupled with changes to the laser's width, shape and intensity as the beam passes through different regions of the laser unit and laser sheet generating componentry. Therefore experimental misalignments not only combine the shift and width variations tested in simulation cases 1 and 2, but also introduce unsimulated parameter variations in profile shape and intensity which are beyond the scope of this study. These additional factors clearly influence both the A_r and resulting $\bar{R}_C$ of the PIV results, explaining the scatter in the data shown in figure 7. Irrespective of these extraneous variables however, the decreasing trend in $\bar{R}_C$ with lower area ratios is consistent with trends observed in the simulation results discussed in Section 2.

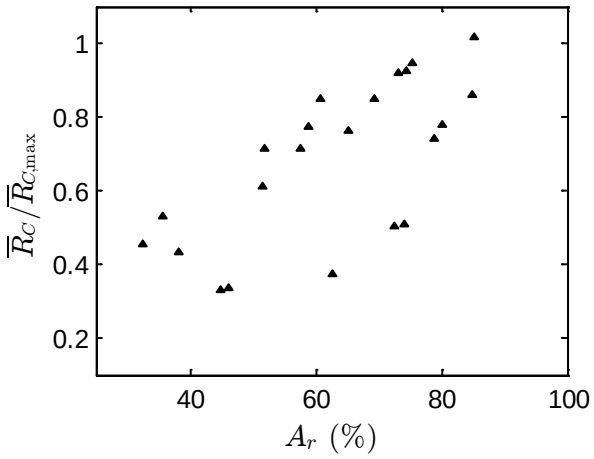

Fig. 7 Experimental normalised mean correlation coefficient

5. Conclusions

A systematic investigation of laser light sheet overlap and profile mismatch has been presented, considering the impacts of shift and width changes on a light sheet between successive PIV pulses. Results reveal the rapid degradation of correlation quality as the two laser profiles used to capture an image pair are no longer well matched. This trend is also reinforced by experimental measurements involving deliberate misalignment of a PIV laser. Furthermore, these data illustrate the complex coupled interactions between the laser mismatch parameters which arise in experiments and can potentially exacerbate the impacts on correlation quality. A modular laser profiling camera design is also outlined to enable high resolution analysis of these behaviours in PIV experiments. Additional applications of this camera system for laser monitoring and diagnostics have been presented. With the use of this laser profiling tool, laser based experimental techniques such as PIV can be setup and refined more rapidly, to achieve better laser alignment and high quality measurement results.

6. Acknowledgements

The authors wish to thank Dougal Squire for his assistance and advice with this study, as well as the financial support of the Australian Research Council.

7. References

Andrèbe Y, Behn R, Duval BP, Etienne P, Pitzschke A (2011) Use of webcams as tools for alignment and supervision of a Thomson scattering system in the near infrared. Fusion Engineering and Design, 86:6:1273-1276.

Blinde PL, Lynch KP, Schrijer FFJ, van Oudheusden BW (2015) Determination of instantaneous pressure in a transonic base flow using four-pulse tomographic PIV. In *Proceedings of the 11th International Symposium on Particle Image Velocimetry*.

Brücker C, Hess D, Kitzhofer J (2012) Single-view volumetric PIV via high-resolution scanning, isotropic voxel restructuring and 3D least-squares matching (3D-LSM). Meas Sci and Technol, 24:2:024001.

Cignoli F, De Iuliis S, Zizak G (2004) A webcam as a light probe beam profiler. Applied spectroscopy, 58:11:1372-1375.

de Silva CM, Baidya R, Khashehchi M, Marusic I (2012) Assessment of tomographic PIV in wall-bounded turbulence using direct numerical simulation data. Exp Fluids, 52:2:425-440.

de Silva CM, Squire DT, Hutchins N, Marusic I (2015) Towards capturing large scale coherent structures in boundary layers using particle image velocimetry. In *Proceedings of 7th Australian conference on laser diagnostics in fluid mechanics and combustion*.

Elsinga GE, van Oudheusden BW, Scarano F (2006) Experimental assessment of tomographic-PIV accuracy. In *Proceedings of the 13th international symposium on applications of laser techniques to fluid mechanics*, 20.

Fond B, Abram C, Beyrau F (2015) On the characterisation of tracer particles for thermographic particle image velocimetry. Applied Physics B, 118:3:393-399.

Ganapathisubramani B, Longmire EK, Marusic I, Pothos S (2005) Dual-plane PIV technique to determine the complete velocity gradient tensor in a turbulent boundary layer. Exp Fluids, 39:2:222-231.

Kähler CJ, Kompenhans J (2000) Fundamentals of multiple plane stereo particle image velocimetry. Exp Fluids, 29:1:S070-S077.

Langer G, Hochreiner A, Burgholzer P, Berer T (2013) A webcam in Bayer-mode as a light beam profiler for the near infra-red. Optics and lasers in engineering, 51:5:571-575.

Mistry D, Dawson J (2014) Experimental investigation of multi-scale entrainment processes of a turbulent jet. In *Proceedings of 17th international symposium on application of laser techniques to fluid mechanics*.

Mullin JA, Dahm WJ (2005) Dual-plane stereo particle image velocimetry (DSPIV) for measuring velocity gradient fields at intermediate and small scales of turbulent flows. Exp Fluids, 38:2:185-196.

Naka Y, Tomita K, Shimura M, Fukushima N, Tanahashi M, Miyauchi T (2016) Quad-plane stereoscopic PIV for fine-scale structure measurements in turbulence. Exp Fluids, 57:5:1-20.

Nickels TB, Marusic I, Hafez S, Chong MS (2005) Evidence of the k 1− 1 law in a high-Reynolds-number turbulent boundary layer. Physical Review Letters, 95:7:074501.

Nobach H, Bodenschatz E (2009) Limitations of accuracy in PIV due to individual variations of particle image intensities. Exp Fluids, 47:1:27-38.

Nobach H (2011) Influence of individual variations of particle image intensities on high-resolution PIV. Exp Fluids, 50:4:919-927.

Pfadler S, Dinkelacker F, Beyrau F, Leipertz A (2009) High resolution dual-plane stereo-PIV for validation of subgrid scale models in large-eddy simulations of turbulent premixed flames. Combustion and Flame, 156:8:1552-1564.

Scarano F, Elsinga GE, Bocci E, van Oudheusden BW (2006) Investigation of 3-D coherent structures in the turbulent cylinder wake using Tomo-PIV. In *Proceedings of the 13th international symposium on applications of laser techniques to fluid mechanics*, 20.

Scharnowski S, Kähler CJ (2016) Estimation and optimization of loss-of-pair uncertainties based on PIV correlation functions. Exp Fluids, 57:2:1-11.

Sillero JA, Jiménez J, Moser RD (2013) One-point statistics for turbulent wall-bounded flows at Reynolds numbers up to $\delta^+ \approx 2000$. Phys Fluids (1994-present), 25:10:105102.

Westerweel J, Scarano F (2005) Universal outlier detection for PIV data. Exp Fluids, 39:6:1096-1100.

Wieneke B (2005) Stereo-PIV using self-calibration on particle images. Exp Fluids 39:2:267-280.